available at www.sciencedirect.com
journal homepage: www.europeanurology.com

European Association of Urology

Surgery in Motion

Three-dimensional Augmented Reality Robot-assisted Partial Nephrectomy in Case of Complex Tumours (PADUA ≥10): A New Intraoperative Tool Overcoming the Ultrasound Guidance

Francesco Porpiglia [a,*], *Enrico Checcucci* [a], *Daniele Amparore* [a], *Federico Piramide* [a], *Gabriele Volpi* [a], *Stefano Granato* [a], *Paolo Verri* [a], *Matteo Manfredi* [a], *Andrea Bellin* [a], *Pietro Piazzolla* [b], *Riccardo Autorino* [c], *Ivano Morra* [a], *Cristian Fiori* [a], *Alex Mottrie* [d,e]

[a] *Division of Urology, Department of Oncology, School of Medicine, University of Turin, San Luigi Hospital, Orbassano, Turin, Italy;* [b] *Department of Management and Production Engineer, Polytechnic University of Turin, Italy;* [c] *Division of Urology, VCU Health, Richmond, VA, USA;* [d] *Onze-Lieve-Vrouw Hospital, Aalst, Belgium;* [e] *OLV Robotic Surgery Institute Academy, Melle, Belgium*

Article info

Article history:
Accepted November 29, 2019

Associate Editor:
Alexandre Mottrie

Keywords:
Three-dimensional reconstruction
Augmented reality
HA3D
Image-guided surgery
Partial nephrectomy
Robotics

Please visit www.europeanurology.com and www.urosource.com to view the accompanying video.

Abstract

Background: Despite technical improvements introduced with robotic surgery, management of complex tumours (PADUA score ≥10) is still a matter of debate within the field of transperitoneal robot-assisted partial nephrectomy (RAPN).
Objective: To evaluate the accuracy of our three-dimensional (3D) static and elastic augmented reality (AR) systems based on hyperaccuracy models (HA3D) in identifying tumours and intrarenal structures during transperitoneal RAPN (AR-RAPN), compared with standard ultrasound (US).
Design, setting, and participants: A retrospective study was conducted, including 91 patients who underwent RAPN for complex renal tumours, 48 with 3D AR guidance and 43 with 2D US guidance, from July 2017 to May 2019.
Surgical procedure: In patients who underwent 3D AR-RAPN, virtual image overlapping guided the surgeon during resection and suture phases. In the 2D US group, interventions were driven by US only.
Measurements: Patient characteristics were tested using the Fisher's exact test for categorical variables and the Mann-Whitney test for continuous ones. Intraoperative, postoperative, and surgical outcomes were collected. All results for continuous variables were expressed as medians (range), and frequencies and proportions were reported as percentages.
Results and limitations: The use of 3D AR guidance makes it possible to correctly identify the lesion and intraparenchymal structures with a more accurate 3D perception of the location and the nature of the different structures relative to the standard 2D US guidance. This translates to a lower rate of global ischaemia (45.8% in the 3D group vs 69.7% in the US group; $p = 0.03$), higher rate of enucleation (62.5% vs 37.5% in the 3D and US groups, respectively; $p = 0.02$), and lower rate of collecting system violation (10.4% vs 45.5%; $p = 0.003$). Postoperatively, 3D AR guidance use correlates to a low risk of surgery-related complications in 3D AR groups and a lower drop in estimated renal plasma flow at renal scan at 3 mo of follow-up (−12.38 in the 3D group vs −18.14 in the US group; $p = 0.01$). The main limitations of this study are short follow-up time and small sample size.
Conclusions: HA3D models that overlap in vivo anatomy during AR-RAPN for complex tumours can be useful for identifying the lesion and intraparenchymal structures that

* Corresponding author. Division of Urology, Department of Oncology, School of Medicine, University of Turin, San Luigi Hospital, Regione Gonzole 10, 10043 Orbassano, Turin, Italy. Tel. +390119026558, Fax: +390119038654.
E-mail address: porpiglia@libero.it (F. Porpiglia).

https://doi.org/10.1016/j.eururo.2019.11.024

are difficult to visualise with US only. This translates to a potential improvement in the quality of the resection phase and a reduction in postoperative complications, with better functional recovery.

Patient summary: Based on our findings, three-dimensional augmented reality robot-assisted partial nephrectomy seems to help surgeons in the management of complex renal tumours, with potential early postoperative benefits.

1. Introduction

Nephron-sparing surgery (NSS) is a widespread treatment for renal cell carcinoma and can be considered the first choice for T1 tumours [1]. Recently, the increasing use of a robotic approach has been advantageous for NSS patients, not only with reduced postoperative pain and morbidity [2], but also with long-term survival, even in T1–T2 cases [3].

Despite technical and technological improvements, management of complex tumours (PADUA score >10 [4]) that have contact with or involvement of intraparenchymal structures such as vessels or calyces, or that are not clearly visible after kidney exposure (endophytic or posteriorly located), still remains an open issue.

In particular, intrarenal tumours present a technical challenge during partial nephrectomy because these lesions cannot be visualised on the kidney surface [5]; moreover, tumours located on the kidney's posterior face [6] require a medialisation and rotation of the kidney before starting the resection phase, in order to expose the lesion, and could be challenging when the kidney is surrounded by "sticky" (adherent perinephric) fat.

Nowadays, different imaging tools have been adopted [7,8] with the aim of improving the quality of NSS and intraoperative surgical navigation. Among them, intraoperative laparoscopic ultrasonography has been widely accepted for tumour identification [9].

Adopting this philosophy, we had already developed a new tool for intraoperative surgical navigation. On the basis of preoperative computer tomography (CT), high-definition three-dimensional (3D) models (hyperaccuracy 3D—"HA3D") of the kidney and tumour were created [10]. Subsequently, thanks to a specifically developed platform, the virtual models overlapped with in vivo anatomy, allowing an augmented reality robot-assisted partial nephrectomy (AR-RAPN) [11].

The aim of this study is to evaluate the accuracy of 3D augmented reality (AR) as intraoperative guidance during RAPN in comparison with standard ultrasound (US-RAPN) in cases of complex tumours, focusing on the capability of each in identifying intraparenchymal structures and driving resection during the two main phases of the surgery: tumour excision and resection bed suture.

2. Patients and methods

2.1. Study population

We researched, for the purpose of this study, prospectively maintained data of all patients with a radiological diagnosis of a complex renal mass who underwent RAPN with intraoperative image guidance at our centre from July 2017 to May 2019.

In cases of complex renal masses, defined as PADUA score ≥10, patients were consecutively enrolled in our study. Once identified, the patients were divided into two groups, based on the different intraoperative guidance used during surgery (US-RAPN or 3D AR-RAPN).

The study was conducted in accordance with good clinical practice guidelines, and informed consent was obtained from the patients. According to Italian law (*Agenzia Italiana del Farmaco* Guidelines for Observational Studies, 20 March 2008), no formal institutional review board or ethics committee approval was needed.

2.2. Three-dimensional virtual model rendering and 3D AR-RAPN

Within 1 mo from the preoperative CT scan date, the images in DICOM format were processed by dedicated software, authorised for medical use by MEDICS Srl (www.medics3d.com), in order to perform the HA3D reconstruction already described [9]. The final output was in STL format.

A specific system was used to overlay virtual data on the endoscopic video, displayed by a remote da Vinci surgical console (Intuitive, Sunnyvale, CA, USA).

The HA3D virtual model of the kidney was loaded into the specifically engineered rViewer application. This software was developed using the Unity platform [12] and C Sharp [13], and was designed to display a 3D model of a patient's kidney, and to control its translation, rotation, and scale transformation values using a 3D professional mouse (Fig. 1A).

In order to simulate tissue deformations occurring during the dynamic phases of the intervention, nonlinear parametric deformations were applied to the 3D model meshes. In particular, as we already described for prostate cancer surgery [14], bend and stretch deformers were selected. All these transformations were described along one main axis and could be combined to obtain deform effects (Fig. 1B).

Then, the video rendered by the rViewer application was mixed with the video taken by the endoscopic camera, using a software video mixer application. The resulting stream was finally sent back to the da Vinci remote console monitor in real time, where it was used by the surgeon as needed, by means of TilePro multi-input display technology. All RAPN procedures were performed by a single highly experienced robotic surgeon (F.P.). Our markers for driving a precise manual overlapping were the kidney boundaries and the

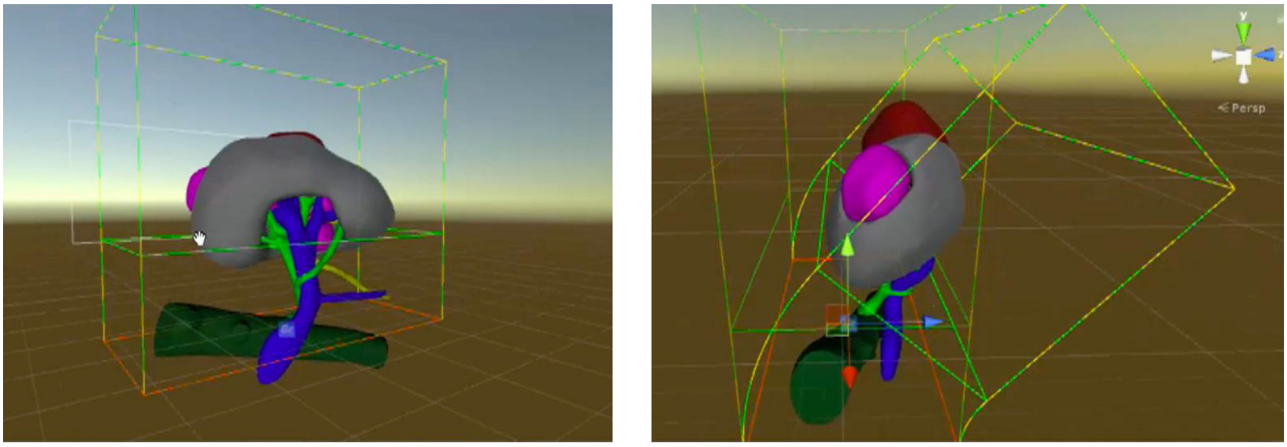

a b

Fig. 1 – (A) Three-dimensional virtual model powered by Unity engine and (B) 3D virtual model with the application of non-linear parametric deformations (bend and stretch). 3D = three dimensional.

renal pedicle. When we modulated the transparency of the 3D virtual models, the renal masses were visualised, even in their deepest and hidden portions. Using the bend and stretch deformers, the superimposed 3D virtual model was stretched and bent following tractions exercised on the kidney by the robotic arms, allowing for a dynamic chasing of kidney movement and deformation during the procedure.

During the intervention, after kidney exposure, thanks to the overlapped 3D AR images and their transparency modulation, the lesion was identified, and its relationships with vessels and calyces were analysed (Fig. 2). In cases of posteriorly located tumours, the bend and stretch deformers were applied in order to follow the in vivo anatomy during kidney rotation (Fig. 3).

Specifically for totally endophytic tumours, a robotic monopolar scissor was used to mark the tumour projection circumferentially on the kidney surface, using the AR. Then the images were double-checked by US. Finally, the extirpative phase started. The branch or branches of the renal artery contacting the tumour, at HA3D reconstruction and confirmed in in vivo anatomy, were clamped by Bulldog.

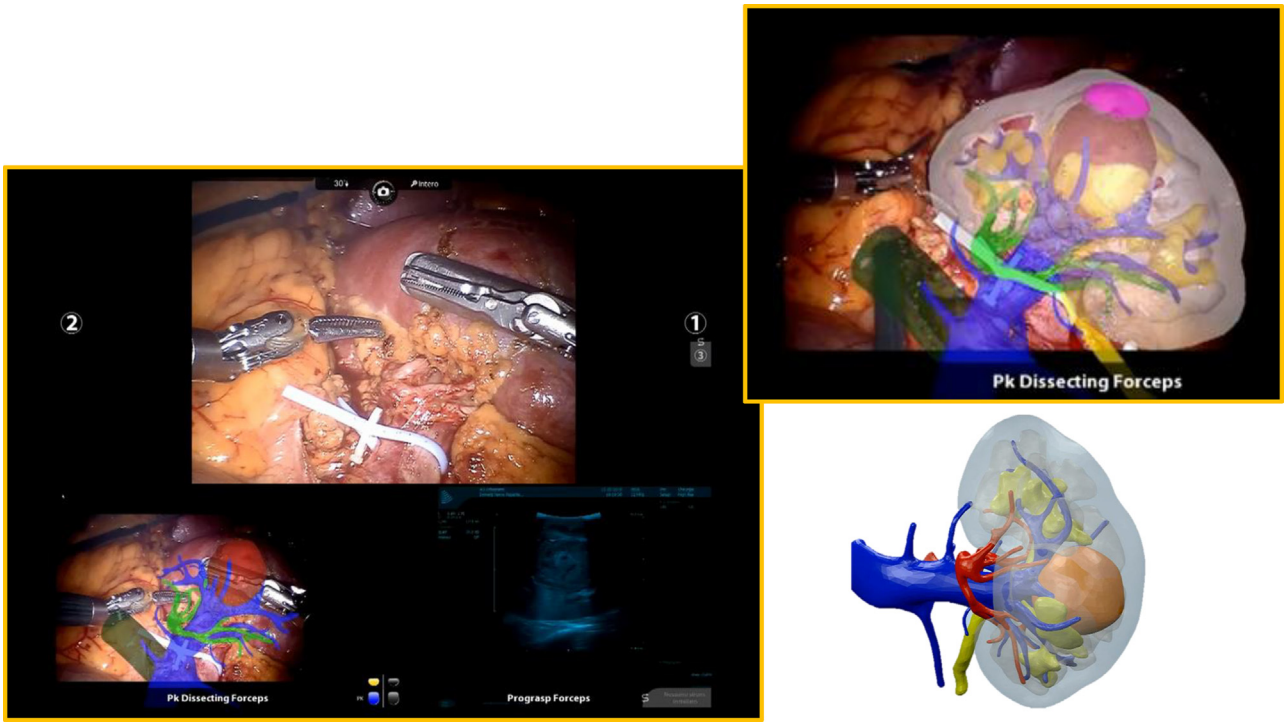

Fig. 2 – For endophytic renal masses, overlapping of augmented reality images on in vivo anatomy enhanced the perception of the lesion location and its relationship with intraparenchymal vessels and calyxes.

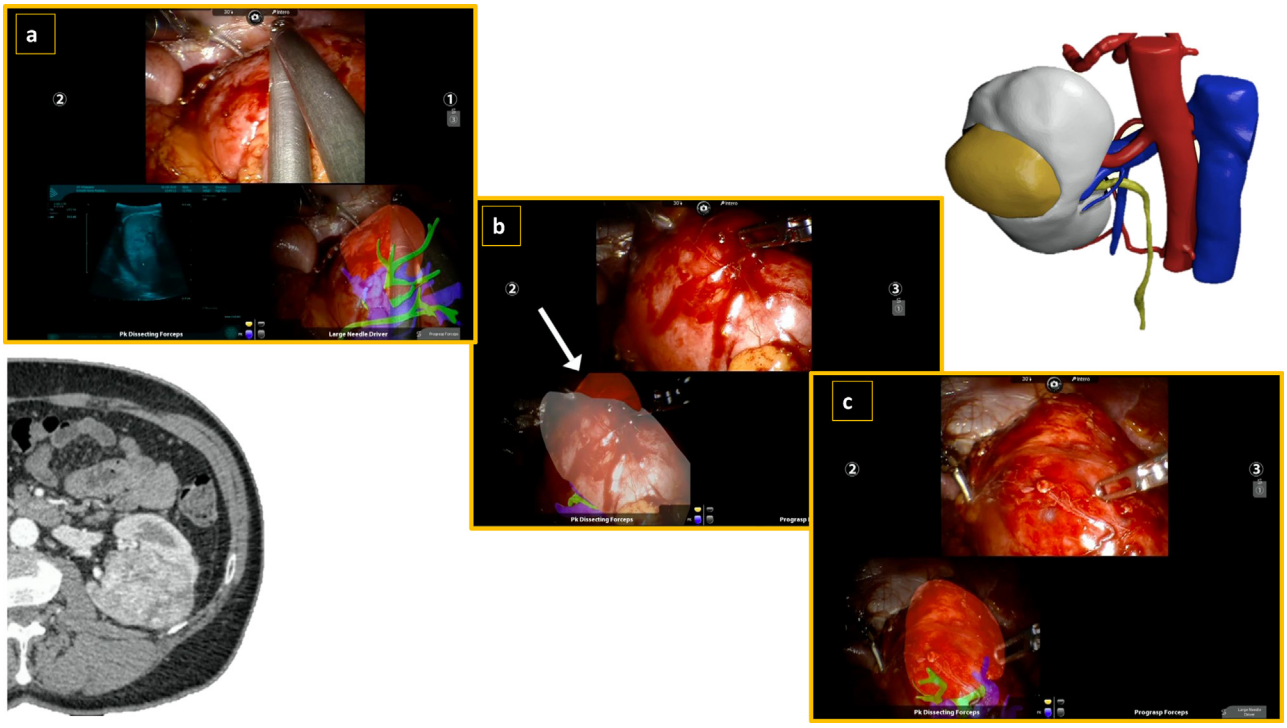

Fig. 3 – (A) Before kidney rotation, the lesion location was identified by AR images and confirmed with US. (B) During kidney rotation, the lesion arose from the posterior face. (C) After kidney rotation, the lesion location was identified with AR images. AR = augmented reality; US = ultrasound.

Subsequently, enucleoresection or enucleation was carried out according to clinical indication. During this phase, in case of identification of perilesional arteries feeding the tumour, a selective clipping with ABSOLOK clips was performed, in order to keep the tumour bed as clean as possible. After tumour removal and complete resective bed exposure, selective sutures of calyces and veins violated during the tumour resection were performed under 3D AR guidance (Fig. 4). Finally, a double layer suture was performed and RAPN was completed [15].

2.3. *US-guided RAPN*

As the realisation of 3D models required 4–6 h of work by the bioengineers, and their presence was always required during surgery, sometimes the arrangement of 3D AR was not possible due to organisational reasons. In such cases, the patients included in this study were scheduled for 2D US procedures.

Similar to the other image guidance tools during RAPN, US was used to identify the location of the tumour, focusing

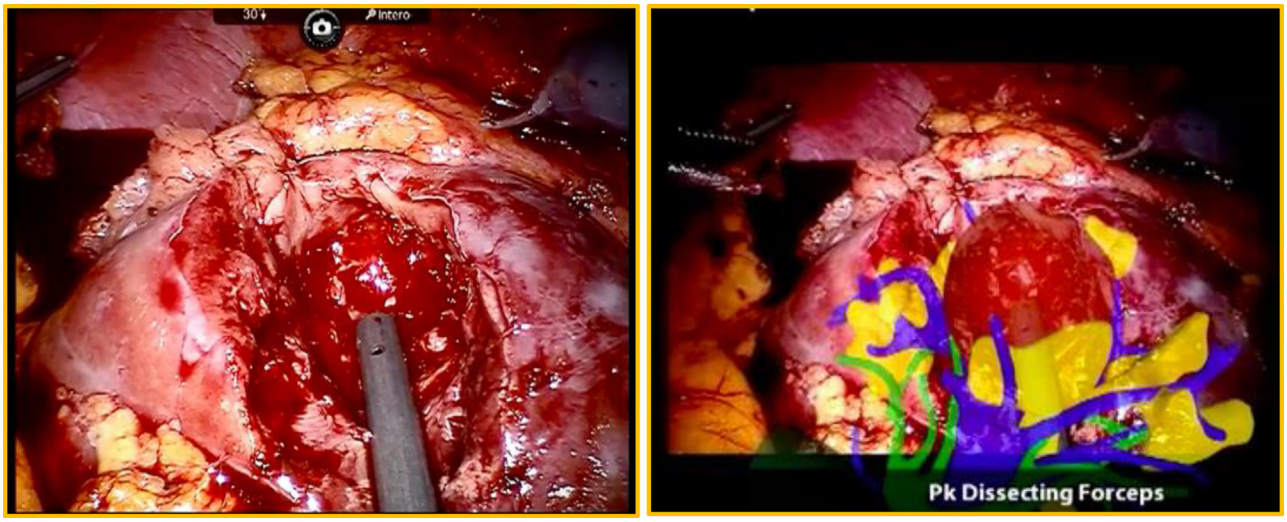

Fig. 4 – After tumour removal, the AR image was overlapped again. The vessels and calyxes emerging from the resection bed and the virtual tumour were clearly visible. AR = augmented reality.

on its boundaries and relationships with the intraparenchymal structures (vessels and calyces) using both standard US and Doppler US, again thanks to the TilePro (BK Robotic Drop-In US Transducer 8826).

The robotic US probe was introduced to the surgical field by the assistant, but its manoeuvre was performed by the surgeon alone, achieving difficult angles while maintaining perpendicular contact between the probe and the kidney surface [16].

2.4. Data analysis

Data collected from the US-RAPN and 3D AR-RAPN groups included the following: demographics including age, body mass index, and comorbidities classified according to the Charlson comorbidity index [17]; clinical size, side, location, and complexity of tumours according to PADUA score [4]; perioperative data (including management of the renal pedicle, and type and duration of ischaemia); pathological data (including stage according to TNM [18]); and postoperative complications as classified according to the Clavien system [19]. Patients with a final diagnosis of renal cell carcinoma underwent oncological follow-up, based on abdominal evaluation using US or CT scan on the basis of disease malignancy. As for functional assessments, an evaluation of serum creatinine (SCr) and estimated glomerular filtration rate (eGFR) was performed preoperatively, both at discharge and 3 mo after surgery. Moreover, all the patients underwent renal scan before and 3 mo after RAPN, and estimated renal plasma flow (ERPF) and split renal function (SRF) were recorded.

In order to evaluate the two different techniques, perioperative data (such as type and time of clamping, type of resection, rate of calyceal system opened, and complication rate) and postoperative data (such as functional outcomes and renal scan results) were collected and compared.

2.5. Statistical analysis

Patient characteristics were tested using Fisher's exact test for categorical variables and the Mann-Whitney test for continuous ones. All results for continuous variables were expressed as medians (range), and frequencies and proportions were reported as percentages. To verify the comparability between the 3D AR-RAPN and US-RAPN groups, baseline variables were evaluated, testing the differences in quantitative and categorical variables with nonparametric Mann-Whitney and chi-square tests, respectively. Data were analysed by StatSoft v.10.

3. Results

A total of 91 patients with a diagnosis of complex renal mass treated with image-guided RAPN were identified and retrospectively analysed. Forty-eight patients underwent 3D AR-RAPN, whilst 43 patients underwent US-RAPN. There were no differences at baseline variables between the two groups (Table 1).

The median (standard deviation) tumour sizes were 48.57 (18.6) and 44.6 (13.1) mm ($p = 0.24$), with median (interquartile range) PADUA scores of 11 (10–12) and 10 (10–11), for the 3D AR and US groups, respectively ($p = 0.65$). No differences were found in operative time (111 vs 128 min; $p = 0.21$), and only one patient was converted to radical nephrectomy in both groups (Table 2).

Focusing on ischaemia techniques, 22 (45.8%) and 30 (69.7%) patients underwent global ischaemia in the 3D AR and US groups, respectively ($p = 0.03$), whilst 21 (44.6%) and eight (18.6%) patients ($p = 0.15$), respectively, received selective clamping of second-order arterial branches of the renal artery for each group (only five clampless procedures were performed in both groups; $p = 0.87$).

The mean ischaemia time for global clamping was 23.2 (7.6) and 24.5 (9.1) min ($p = 0.45$), whilst for selective clamping, it was 22.5 (8.9) and 23.6 (5.3) min, respectively ($p = 0.48$).

In the 3D AR group, 30 patients (62.5%) underwent enucleation, whilst enucleoresection was performed in 18 (37.5%); on the contrary, in the US group, 16 (37.2%) enucleations and 27 (62.8%) enucleoresections were performed ($p = 0.02$).

The collecting system was violated in five patients in the 3D AR-RAPN group (10.4%) and 20 patients in the US-RAPN group (46.5%; $p = 0.003$).

Blood loss volumes were 179.3 ml (132.1) and 182.5 ml (158.4) in the 3D and US groups, respectively ($p = 0.91$). Transfusions were needed in one (2.3%) and five (11.6%) patients in the 3D and US groups, respectively ($p = 0.17$).

No intraoperative complications occurred in either group.

Overall, the postoperative complication rates were 18.7% and 18.6% in the 3D and US groups, respectively ($p = 0.79$).

One Clavien $\geq$3 complication was recorded in the 3D AR group (myocardial infarction that required revascularisation), whilst two Clavien $\geq$3 complications occurred in the US group ($p = 0.93$).

With regard to the subanalysis of complications potentially related to the quality of the resection and to the suture of intrarenal structures violated during the extirpative phase, only one case of postoperative bleeding, not requiring reintervention, occurred in the 3D AR group. However, in the US group, three complications were recorded: one urinary fistula that required urinary stent application, one postoperative bleeding treated with selective embolisation, and one haematoma that was managed conservatively ($p = 0.20$).

The functional outcome evaluation showed postoperative worsening of Δ SCr equal to 18.2% and 23.6% ($p = 0.06$), with Δ eGFR values of –14.26% and –19.46% ($p = 0.11$), in the 3D and US groups, respectively.

When the kidney was treated with robotic surgery only, Δ SRF values were –10.83 and –4.10 ($p = 0.38$), whilst Δ ERPF values were –12.38 and –18.14 in the 3D AR and US groups ($p = 0.01$), respectively (Table 3).

Two (4.2%) and two (4.6%; $p = 0.67$) positive surgical margins, respectively, were recorded in the two groups. Taking into account the limits of extremely short follow-up (3 mo), no recurrences were recorded (Table 4).

Table 1 – Descriptive analysis of preoperative features.

Preoperative features		3D AR-RAPN	2D US-RAPN	*p* value
Number of patients		48	43	
Males, no. (%)		35 (72.9)	33 (76.7)	0.86
Age (yr), mean (SD)		62 (15)	58 (9.8)	0.14
BMI (kg/m2), mean (SD)		24.1 (3.7)	25.9 (3.8)	0.02
CCI, median (IQR)		1 (0–2)	1 (0–2)	1.00
CCI age adjusted, median (IQR)		4 (2–4)	4 (2–4)	1.00
ECOG, median (IQR)		0 (0–1)	0 (0–1)	1.00
ASA score, median (IQR)		2 (1–2)	2 (1–2)	1.00
Preoperative haemoglobin (mg/dl), mean (SD)		13.9 (1.5)	14.4 (1.5)	0.11
Solitary kidney, no. (%)		4 (8.3)	5 (11.6)	0.86
CT lesion size (mm), mean (SD)		48.57 (18.67)	44.6 (13.1)	0.24
Tumour right side, no. (%)		28 (58.3)	18 (41.8)	0.17
Clinical stage, no. (%)	cT1a	21 (43.8)	19 (44.2)	0.86
	cT1b	22 (45.8)	22 (51.2)	0.76
	>cT2	5 (10.4)	2 (4.6)	0.51
Tumour location, no. (%)	Polar sup	13 (27.1)	8 (18.6)	0.47
	Mesorenal	23 (47.9)	24 (55.8)	0.58
	Polar inf	12 (25.0)	11 (25.5)	0.85
Tumour growth pattern, no. (%)	>50% exophytic	14 (29.2)	7 (16.3)	0.22
	<50% exophytic	19 (39.6)	23 (53.4)	0.26
	Endophytic	15 (31.2)	13 (30.2)	0.90
Kidney face location, no. (%)	Anterior face	28 (58.3)	31 (72.1)	0.24
	Posterior face	20 (41.7)	12 (27.9)	0.24
Kidney rim location, no. (%)	Lateral margin	28 (58.3)	12 (27.9)	0.006
	Medial margin	20 (41.7)	31 (72.1)	0.006
CT-based PADUA score, median (IQR)		11 (10–12)	10 (10–11)	0.65
3D-based PADUA score, median (IQR)		10 (9–11)	//	NA

AR = augmented reality; ASA = American Society of Anesthesiologists; BMI = body mass index; CCI = Charlson comorbidity index; CT = computed tomography; ECOG = Eastern Cooperative Oncology Group; inf = inferior; IQR = interquartile range; RAPN = robot-assisted partial nephrectomy; SD = standard deviation; sup = superior; US = ultrasound; 2D = two dimensional; 3D = three dimensional.

Table 2 – Intraoperative variables.

Intraoperative variables		3D AR-RAPN	2D US-RAPN	*p* value
Hilar clamping, no. (%)	Global ischaemia	22 (45.8)	30 (69.7)	0.03
	Selective ischaemia	21 (44.6)	8 (18.6)	0.15
	Clampless	5 (10.4)	5 (11.6)	0.87
Ischaemia time (min), mean (SD)	Global ischaemia	23.2 (7.6)	24.5 (9.1)	0.45
	Partial ischaemia	22.5 (8.9)	23.6 (5.3)	0.48
EBL (cc), mean (SD)		179.3 (132.1)	182.5 (158.4)	0.91
Operative time (min), mean (SD)		110.9 (72.5)	128.4 (59.5)	0.21
Transfusion rate, no. (%)		1 (2.3)	5 (11.6)	0.17
Extirpative technique, no. (%)	Enucleations	30 (62.5)	16 (37.2)	0.02
	Enucleoresections	18 (37.5)	27 (62.8)	0.02
Opening collecting system, no. (%)	Yes	5 (10.4)	20 (46.5)	0.0003
	No	43 (89.6)	23 (53.4)	0.0003
Conversion to radical nephrectomy, no. (%)		1 (2.1)	0 (0)	0.96
Intraoperative complications, no. (%)		0 (0)	0 (0)	NA
Postoperative complications, no. (%)		9 (18.7)	8 (18.6)	0.79
Postoperative complication according to Clavien-Dindo, no. (%)	<3	8 (16.7)	6 (13.9)	0.93
	≥3	1 (2.1)	2 (4.6)	0.93
Complication surgery related	Total	1 (2.1)	3 (6.9)	0.20
	Urinary fistula	0 (0)	1 (2.1)	0.96
	Postoperative bleeding treated with embolisation	0 (0)	1 (2.1)	0.96
	Postoperative haematoma	0 (0)	1 (2.1)	0.96

AR = augmented reality; EBL = estimated blood loss; NA = not available; RAPN = robot-assisted partial nephrectomy; SD = standard deviation; US = ultrasound; 2D = two dimensional; 3D = three dimensional.

4. Discussion

The main goal of NSS is, together with oncological safety, to minimise the sacrifice of healthy perilesional parenchyma, leaving as many uninjured nephrons as possible to guarantee maximal functional recovery while preserving intraparenchymal structures (vessels and calyxes). In fact, it is well known and accepted that the reduction of unaffected nephrons is related to worse cancer-specific mortality [20] and loss of renal function, due to the decrease in renal volume [21–23].

Table 3 – Functional variables.

Functional variables	3D AR-RAPN	2D US-RAPN	*p* value
Preoperative SCr (mg/dl), mean (SD)	1.11 (0.69)	0.97 (0.28)	0.21
Preoperative eGFR (ml/min), mean (SD—MDRD formula)	78.9 (27.65)	85.1 (21.47)	0.23
Postoperative SCr (mg/dl), mean (SD)	1.36 (0.92)	1.20 (0.51)	0.31
Postoperative eGFR (ml/min), mean (SD—MDRD formula)	66.6 (26.37)	69.9 (19.75)	0.50
Δ SCr (%)	18.2	23.6	0.06
Δ eGFR (%)	−14.26	−19.46	0.11
Preoperative split renal function, mean (SD)	44.11 (12.76)	53.27 (16.53)	0.003
Postoperative split renal function, mean (SD)	40.67 (11.73)	46.16 (19.26)	0.10
Preoperative ERPF, mean (SD)	198.63 (48.87)	198.12 (69.36)	0.96
Postoperative ERPF, mean (SD)	152.58 (55.06)	153.18 (64.91)	0.96
Δ Split renal function (%)	−10.83	−14.10	0.38
Δ ERPF (%)	−12.38	−18.14	0.01

AR = augmented reality; eGFR = estimated glomerular filtration rate; ERPF = effective renal plasmatic flow; RAPN = robot-assisted partial nephrectomy; SCr = serum creatinine; SD = standard deviation; US = ultrasound; 2D = two dimensional; 3D = three dimensional.

Table 4 – Histopathological findings.

Pathological findings		3D AR-RAPN	2D US-RAPN	*p* value
Pathological stage, no. (%)	Benign	8 (16.6)	5 (11.6)	0.70
	pT1a	14 (29.2)	10 (23.2)	0.001
	pT1b	19 (39.6)	20 (46.5)	0.65
	pT2	2 (4.2)	2 (4.6)	0.67
	pT3	5 (10.4)	6 (13.9)	0.84
Pathological size (mm), mean (SD)		47.84 (17.38)	44.5 (13.9)	0.31
Positive surgical margin rate, no. (%)		2 (4.2)	2 (4.6)	0.67
Histopathological findings, no. (%)	Clear cell carcinoma	35 (87.5)	28 (65.1)	0.02
	Papillary	3 (7.5)	4 (9.3)	0.94
	Chromophobe	1 (2.5)	3 (6.9)	0.61
	Oncocytoma	0 (0)	4 (9.3)	0.09
	Angiomyolipoma	0 (0)	2 (4.6)	0.43
	Unclassified	0 (0)	1 (2.3)	0.96
	Others	1 (2.5)	1 (2.3)	0.96
ISUP grade, no. (%)	1	5 (12.5)	6 (13.9)	0.12
	2	22 (55)	20 (46.5)	0.55
	3	11 (27.5)	9 (20.9)	0.62
	4	0 (0)	0 (0)	NA
	Not applicable	2 (5.0)	8 (18.6)	0.08

AR = augmented reality; ISUP = International Society of Urological Pathology; NA = not available; RAPN = robot-assisted partial nephrectomy; SD = standard deviation; US = ultrasound; 2D = two dimensional; 3D = three dimensional.

At present, surgery is becoming ever more precise [24], and image-guided interventions are crucial [8] to optimise procedure tailoring, with the goal of maximising functional outcomes without compromising on oncological safety.

Nowadays, it is even possible to obtain 3D reconstructions of every single case studied from preoperative imaging such as CT scans. As we have already demonstrated in a previous study, thanks to a collaboration between urologists and bioengineers, hyperaccurate reconstructions (HA3D models) of the kidney and its internal structures can be realised [11].

The role of these 3D virtual models, in particular in preoperative planning [10] and intraoperative decision making, is now widely accepted [11]. Our data confirmed again that preoperative planning based on 3D models allows for a better understanding of vascular anatomy, reducing the rate of global clamping significantly (70% vs 46%, $p = 0.03$). The wider use of selective clamping in our series does not reach statistical significance—maybe due to the small simple size—but a favourable trend was shown.

The newest field of application of these models focuses on the overlapping of virtual reconstructions on real anatomy during surgical procedures, yielding AR procedures.

For NSS, the preliminary results of the clinical application of this new technology are very encouraging because of the potential to improve both oncological and functional outcomes of partial nephrectomy [25,26].

In order to make a personal contribution to this field, we created a dedicated platform for AR-RAPN.

One of the challenges of AR is image registration of the overlay. In order to maximise the accuracy of the superimposition, we opted for manual registration. Manual superimposition was performed by two assistants, each with experience in >20 cases prior to the beginning of this study.

The overlapped 3D virtual reconstructions were used in order to simplify identification of complex tumours, especially endophytic or posteriorly located ones. Intraoperatively, we had visual feedback of the accuracy of the

overlap. After kidney exposure, the virtual renal pedicle perfectly corresponded to the real vascular pedicle, and the landmarks of the virtual kidney perfectly corresponded to the real one. Modulation of the transparency of the virtual model allowed us not only to visualise the hidden endophytic tumour through the parenchyma, but also to identify the intraparenchymal structures, such as vessels and calyces, close to the tumours.

A step further in the development of our technology was made with the study of complex biomechanical modelling options [27] and the application of nonlinear parametric deformations, in order to approximate target organ deformation and simulate tissue deformation during the intervention, both of which are particularly useful in cases of posterior renal masses.

In its current state, this technology seems to allow essentially a "visual" level of accuracy, guaranteed by surgeon and assistant experience. A mathematical evaluation of the accuracy level is currently being investigated and will be the topic of future research.

As regards the aim of the study specifically, the comparison of the 3D AR technology with the US guidance surgery, in terms of feasibility and usefulness, made the differences between the two intraoperative imaging tools clear.

Concerning lesion identification, in all cases, the overlap of 3D virtual AR images correctly identified tumour location. Moreover, tumour contouring with monopolar scissors on the kidney surface, driven by overlapped AR images, was used to drive the resection. In the case of posteriorly located lesions, the 3D elastic AR images correctly identified and simulated tissue deformation during kidney mobilisation. The use of 3D AR images particularly permitted early and progressive identification of the lesion, especially when not completely exophytic, rising from the kidney surface during the organ rotation. After partial mobilisation of the kidney, the elastic 3D model allowed early identification of the lesion before its appearance on the organ surface. Therefore, the assistance of 3D AR images, in 40% of lesions, made it possible to avoid a complete rotation of the kidney, without compromising the resection.

By visualising the endophytic tumours using TilePro and AR images, the surgeon can have more freedom in surgical action, without needing to manoeuvre the US probe, potentially increasing confidence in tumour excision and 3D perception of the lesion features. This should result in a more accurate resection phase, guided step by step by AR images. All this translates to a higher rate of enucleation in the 3D AR group than in the US group ($p = 0.02$), and to a higher percentage of healthy preserved parenchyma. The pure enucleation technique made it possible to stay closer to the lesion, reducing the depth of healthy parenchyma sacrificed; indirectly, this more precise resection could be related to a lower rate of opening of the collecting system (10.4% vs 46.5% in the 3D and US groups, respectively; $p = 0.0003$).

During the resection phase, the use of 3D AR images permitted visualisation of the intraparenchymal arteries and veins contacting the tumour in order to plan selective management strategies.

In addition, collecting system structures were identified beyond the kidney surface, allowing the surgeon to understand their distribution and potential involvement with the tumour.

The same structures were visualised at the level of resection bed after tumour excision, and further selective management with dedicated sutures in case of violation was performed. Concerning the aid given by US intraoperative guidance during these steps of the surgery, the probe, manoeuvred by the surgeon, was able to identify tumour boundaries and some calyceal and sinusal structures. With the use of Doppler modality, some intraparenchymal perilesional vessels were also identified. However, US did not allow the surgeon to perceive the precise location of all these structures; its images were displayed relative to the ultrasonographic beam diffusion field only. In order to increase the perception of visualised structures, the surgeon had to look constantly at the position of the US probe. An attempt at US image guidance was also performed after tumour removal, often with the kidney under warm ischaemia, to identify the intrarenal structures (vessels and calyces) emerging from the resection bed and potentially violated during tumour excision. However, the precise anatomical structures of the calyces were difficult to determine, and it was impossible to assess the precise location and nature of the vessels, the main renal artery often being still clamped. Finally, the ultrasonographic images were suboptimal, due to the interposition of a blood slice between the resection bed surface and the US probe.

In summary, the use of 3D AR guidance during RAPN, tailored to the specific anatomy of the intraparenchymal structures, allowed optimisation of the outcomes of both extirpative and reconstructive phases of the surgery; US guidance, on the contrary, turned out to be useful only for some outcomes of the extirpative phase.

This surgical outcome optimisation translates to risk minimisation for surgery-related postoperative complications. In fact, in the 3D AR group, no patient developed postoperative bleeding requiring selective embolisation, whilst in the US group, one patient required selective embolisation and another developed a postoperative haematoma that was managed conservatively.

Focusing on the postoperative complications related to the urinary collecting system violation, one patient required urinary stent application due to urinary fistula in the US group. However, no postoperative urine leakages were recorded in the 3D AR group, with evidence suggesting that effective suturing of the violated calyceal structures had been performed. Together with the reduced risk of developing postoperative complications, the use of 3D AR during RAPN also seemed to have an impact on postoperative renal function. In fact, if the level of SCr and eGFR showed a trend only slightly in favour of the 3D group, their values being affected by the functions of both kidneys. Functional assessment of the operated kidney, as evaluated with renal scintigraphy, showed significant advantages in terms of Δ ERPF (–12.38% in the 3D group and –18.14% in the 2D group; $p = 0.01$).

Despite the promising results of this novel technology in driving a real AR-RAPN, the current study is not devoid of limitations. First, 3D model segmentation of the kidney and tumours was performed manually; an experienced urologist and an experienced radiologist were necessary to complete the segmentation process. Second, the entire process of intraoperative overlapping needs to be driven by an assistant, because the 3D mouse has to be manipulated during the whole procedure, to create proper orientation and deformation of the model. Future evolution of this technology would be an automated model, consolidated to organ movements during the surgery. Moreover, access to more computationally complex techniques, such as those that simulate tissue dynamics, will allow the quality and realism of the deformations to improve. Third, in order to assess final consideration of the real benefit of AR technology relative to the standard US, a prospective randomised study and larger sample sizes are required.

Despite the limitations, this study is the first to evaluate the role of AR in the setting of RAPN. With the aid of this new technology, it is possible not only to correctly identify the tumours even when they have hidden locations, but also to visualise the intraparenchymal structures contacting the tumour that can be violated during the surgery. All this yields a potential improvement in the quality of the resection and of the suture of tumour bed, as well as a reduction in postoperative complications and renal damage.

5. Conclusions

Our findings suggest that HA3D kidney virtual reconstruction, based on CT data and real-time superimposed imaging, allows surgeons to perform an effective AR-RAPN for complex tumours.

This technology can be useful for identifying the intraparenchymal structures that are difficult to visualise with US only. This translates to a potential improvement in the quality of the resection phase and a slight reduction of postoperative complications, with better functional recovery.

***Author contributions*:** Francesco Porpiglia had full access to all the data in the study and takes responsibility for the integrity of the data and the accuracy of the data analysis.
Study concept and design: Porpiglia.
Acquisition of data: Granato, Verri.
Analysis and interpretation of data: Piramide, Volpi.
Drafting of the manuscript: Checcucci, Amparore.
Critical revision of the manuscript for important intellectual content: Fiori, Manfredi, Autorino, Morra.
Statistical analysis: Checcucci, Autorino.
Obtaining funding: None.
Administrative, technical, or material support: Piazzolla, Bellin.
Supervision: Porpiglia, Mottrie.
Other: None.

Financial disclosures: Francesco Porpiglia certifies that all conflicts of interest, including specific financial interests and relationships and affiliations relevant to the subject matter or materials discussed in the manuscript (eg, employment/affiliation, grants or funding, consultancies, honoraria, stock ownership or options, expert testimony, royalties, or patents filed, received, or pending), are the following: None.

Funding/Support and role of the sponsor: None.

Appendix A. Supplementary data

Supplementary material related to this article can be found, in the online version, at doi:https://doi.org/10.1016/j.eururo.2019.11.024.

References

[1] Ljungberg B, Bensalah K, Canfield S. EAU guidelines on renal cell carcinoma: 2014 update. Eur Urol 2015;67:913–24.
[2] Poulakis V, Witzsch U, de Vries R, Moeckel M, Becht E. Quality of life after surgery for localized renal cell carcinoma: comparison between radical nephrectomy and nephron-sparing surgery. Urology 2003;62:814–20.
[3] Mir MC, Derweesh I, Porpiglia F, Zargar H, Mottrie A, Autorino R. Partial nephrectomy versus radical nephrectomy for clinical T1b and T2 renal tumors: a systematic review and meta-analysis of comparative studies. Eur Urol 2017;71:606–17.
[4] Ficarra V, Novara G, Secco S, et al. Preoperative aspects and dimensions used for an anatomical (PADUA) classification of renal tumours in patients who are candidates for nephron-sparing surgery. Eur Urol 2009;56:786–93.
[5] Arora S, Rogers C. Partial nephrectomy in central renal tumors. J Endourol 2018;32:S63–7.
[6] Marconi L, Challacombe B. Robotic partial nephrectomy for posterior renal tumours: retro or transperitoneal approach? Eur Urol Focus 2018;4:632–5.
[7] Porpiglia F, Fiori C, Checcucci E, Pecoraro A, Di Dio M, Bertolo R. Selective clamping during laparoscopic partial nephrectomy: the use of near infrared fluorescence guidance. Minerva Urol Nefrol 2018;70:326–32.
[8] Aoun F, Albisinni S, Zanaty M, Hassan T, Janetschek G, van Velthoven R. Indocyanine green fluorescence-guided sentinel lymph node identification in urologic cancers: a systematic review and meta-analysis. Minerva Urol Nefrol 2018;70:361–9.
[9] Qin B, Hu H, Lu Y, et al. Intraoperative ultrasonography in laparoscopic partial nephrectomy for intrarenal tumors. PLoS One 2018;13:e0195911.
[10] Porpiglia F, Bertolo R, Checcucci E, et al. Development and validation of 3D printed virtual models for robot-assisted radical prostatectomy and partial nephrectomy: urologists' and patients' perception. World J Urol 2018;36:201–7.
[11] Porpiglia F, Fiori C, Checcucci E, Amparore D, Bertolo R. Hyperaccuracy three-dimensional reconstruction is able to maximize the efficacy of selective clamping during robot-assisted partial nephrectomy for complex renal masses. Eur Urol 2018;74:651–60.
[12] Unity. https://unity3d.com/.
[13] Microsoft. https://docs.microsoft.com/en-us/dotnet/csharp/language-reference/language-specification/.
[14] Porpiglia F, Checcucci E, Amparore D, et al. Three-dimensional elastic augmented-reality robot-assisted radical prostatectomy using hyperaccuracy three-dimensional reconstruction technology: a step further in the identification of capsular involvement. Eur Urol 2019;76:505–14.
[15] Porpiglia F, Bertolo R, Amparore D, Fiori C. Nephron-sparing suture of renal parenchyma after partial nephrectomy: which technique to go for? Some best practices. Eur Urol Focus 2019;5:600–3.

[16] Kaczmarek BF, Sukumar S, Petros F, et al. Robotic ultrasound probe for tumor identification in robotic partial nephrectomy: Initial series and outcomes. Int J Urol 2013;20:172–6.
[17] Nuttall M, van der Meulen J, Embertona M. Charlson scores based on ICD-10 administrative data were valid in assessing comorbidity in patients undergoing urological cancer surgery. J Clin Epidemiol 2006;59:265–73.
[18] Moch H, Artibani W, Delahunt B, et al. Reassessing the current UICC/ AJCC TNM staging for renal cell carcinoma. Eur Urol 2009;56:636–43.
[19] Dindo D, Demartines N, Clavien PA. Classification of surgical complications: a new proposal with evaluation in a cohort of 6336 patients and results of a survey. Ann Surg 2004;240:205–13.
[20] Antonelli A, Minervini A, Sandri M, et al. Below safety limits, every unit of glomerular filtration rate counts: assessing the relationship between renal function and cancer-specific mortality in renal cell carcinoma. Eur Urol 2018;74:661–7.
[21] Song C, Bang JK, Park HK, Ahn H. Factors influencing renal function reduction after partial nephrectomy. J Urol 2009;181:48–53.
[22] Bertolo R, Zargar H, Autorino R, et al. Estimated glomerular filtration rate, renal scan and volumetric assessment of the kidney before and after partial nephrectomy: a review of the current literature. Minerva Urol Nefrol 2017;69:539–47.
[23] Bertolo R, Fiori C, Piramide F, et al. Assessment of the relationship between renal volume and renal function after minimally-invasive partial nephrectomy: the role of computed tomography and nuclear renal scan. Minerva Urol Nefrol 2018;70:509–17.
[24] Autorino R, Porpiglia F, Dasgupta P, et al. Precision surgery and genitourinary cancers. Eur J Surg Oncol 2017;43:893–908.
[25] Detmer FJ, Hettig J, Schindele D, Schostak M, Hansen C. Virtual and augmented reality systems for renal interventions: a systematic review. IEEE Rev Biomed Eng 2017;10:78–94.
[26] Hughes-Hallett A, Mayer EK, Marcus HJ, et al. Augmented reality partial nephrectomy: examining the current status and future perspectives. Urology 2014;83:266–73.
[27] Payan Y. Soft tissue biomechanical modeling for computer assisted surgery. New York, NY: Springer; 2012. http://dx.doi.org/10.1007/978-3-642-29014-5.